A&A 423, 1171–1177 (2004)
DOI: 10.1051/0004-6361:20034179

Astronomy & Astrophysics

A 230 GHz heterodyne receiver array for the IRAM 30 m telescope

K.-F. Schuster[1], C. Boucher[1], W. Brunswig[1], M. Carter[1], J.-Y. Chenu[1], B. Foullieux[1,2], A. Greve[1], D. John[1], B. Lazareff[1], S. Navarro[1], A. Perrigouard[1], J.-L. Pollet[1], A. Sievers[1], C. Thum[1], and H. Wiesemeyer[1]

[1] IRAM, Institut de Radio-Astronomie Millimétrique, 300 rue de la Piscine, 38406 St Martin d'Hères, France
e-mail: schuster@iram.fr
[2] LAOG, Laboratoire d'Astrophysique de l'Observatoire de Grenoble, 414 rue de la Piscine, 38406 St Martin d'Hères, France

Received 11 August 2003 / Accepted 11 May 2004

Abstract. We describe the technical concept, properties, and performance of HERA (HEterodyne Receiver Array) at the IRAM 30 m telescope. HERA is a multibeam, waveguide SIS receiver that greatly improves mapping speed in various observing modes and also provides possibilities for new high-sensitivity observing of small sources. Future extensions with a second polarization module will permit spectro-polarimetry. We present some examples of astronomical maps with HERA.

Key words. instrumentation: spectrographs – techniques: spectroscopic – radio lines: general

1. Introduction

Array receivers have long been on radio astronomers' wish lists. While focal-plane arrays of bolometer continuum detectors progressed rapidly in the past decade, heterodyne spectral-line arrays encountered difficulties that made progress less rapid. One problem is the sheer complexity of spectral-line receivers: – they need local oscillators, low-noise high-frequency amplifiers, and large spectrometers. Up to now, the ongoing improvement of receiver sensitivity in the millimeter range meant that it was more efficient to enhance the performance of a single beam rather than to add more beams. This changed in recent years. Large multi-channel backends became feasible, and single-beam sensitivity improvements are now slower than before, as receivers approach the "quantum noise", $h\nu/k$, and the atmospheric limits.

The goals of array receivers are faster mapping speed and improved data quality. To make a receiver worth the large effort that goes into building the array, one needs a careful design based on practical and theoretical constraints, the specific telescope to be used, and the astronomy to be done with it. In recent years, SIS array receivers have been installed on mm- and sub-mm telescopes, following quite different technical concepts (Sunada et al. 2000; Klein et al. 2002; Graf et al. 2002). We describe the specific choices that were made for HERA at the IRAM 30 m telescope, and their impact on performance and versatility. Details on numerical models and the design checks by laboratory testing are in Schuster et al. (2000a). Here, we report on the measurement of receiver parameters at the telescope, list possible observing modes, and show examples of maps of astronomical objects.

2. Technical design

HERA was designed to be a robust and reliable facility instrument with long-term standby capabilities. The design of HERA was driven by the fact that 230 GHz is a low enough frequency that high-precision micro-machining can still yield excellent waveguide components. The design therefore uses LO injection and single-sideband SIS mixer units in full waveguide technology. This makes the focal plane units and the whole cryostat extremely compact – an important factor for cryogenics and receiver cabin layout. The quasi-optical part of the receiver is designed for de-rotating the field and re-imaging onto the focal plane units as well as for polarization splitting. We chose an optical design with closely-spaced, dual-polarization beams in a 3×3 pattern, that yields a versatile instrument for both large-scale and small- scale mapping. Due to its symmetry, the 3×3 arrangement greatly reduces the complexity.

2.1. Optics

The optics of HERA satisfies several needs simultaneously (Fig. 1). The K-mirror in front of the cryostat consists of two flats and a central off-axis parabola, that re-images the telescope aperture onto the 9 cm-diameter cryostat window. A similar arrangement has been used for sub-mm bolometer arrays like SCUBA (Gear et al. 1995) and far-IR arrays like FIFI (Poglitsch et al. 1991), but has up to now not been used for mm-array receivers. The cryostat window is high-density polyethylene HDPE with triangular anti-reflection grooves. The cryostat window is followed by a beam-stop IR-filter on the 70 K stage which acts upon stray radiation. The folded

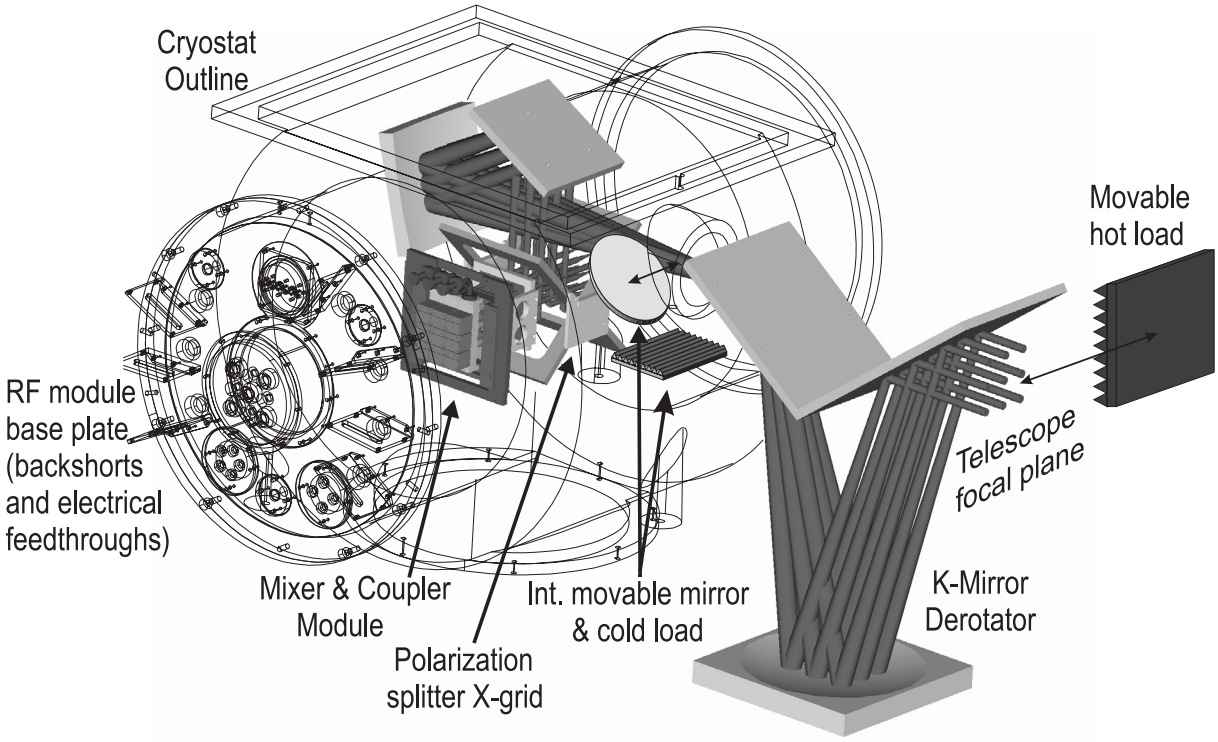

Fig. 1. HERA optical scheme. The mechanical drive of the K-mirror has been omitted for clarity.

internal optics is purely reflective and kept at a temperature of 70 K (except for the plastic lens array at 4.2 K in front of the individual corrugated horns of the mixers). A second off-axis elliptical mirror forms a Gaussian telescope with the off-axis elliptical of the K-mirror. This arrangement reduces the image size by a factor 1.4. The optical train continues via a folding flat onto an X-grid that separates the orthogonal polarizations and directs them into the two plug-in modules. Remaining IR radiation passes straight through the X-Grid falls onto a 70 K absorber.

We decided to use the K-mirror to de-rotate the array image. The mechanical drive is located under the rooftop mirror. Along with the folding angle of 33°, this gives an extremely compact device that can be moved with high speed and precision, without any mechanical stress on the cryostat. The folding angle is a compromise between the lateral size of the derotator (large folding angle) and the need to minimize distortions from the elliptical mirror (small folding angle). To our knowledge, HERA is the first radio receiver to use this kind of derotator; the design has since been adopted by other groups (Brüll 2000). The K-mirror derotator leaves the cryostat in a fixed position, thereby relaxing requirements for mechanical and electrical stability. Without correction, the varying relative alignment of the off-axis elliptical mirrors would strongly distort the image in a variable way. By making the off-axis mirrors more spherical than pure elliptical, while keeping the same effective focal lengths, we were able to reduce this effect without degrading any other optical parameter. After the X-wire grid, the beams pass through a truncated lens array with corrugated surfaces. The lenses re-image the telescope aperture onto the horn apertures, giving optimal beam coupling.

An internal movable mirror allows us to calibrate all beams on an internal cold load on the 70 K structure. The corresponding external hot load is put in front of the K-mirror, close to the telescope focal plane. The losses between the two locations of the calibration loads give an increased effective cold load temperature at the site of the hot load. These losses are nearly independent of frequency, and we verified experimentally that the effective cold load temperature can be calculated directly from the actual physical temperature of the aluminum surface under the absorber, as measured with a high-precision temperature sensor, by applying a single numerical factor (0.8) for all beams. This factor includes the difference between the physical temperature of the aluminum support and the carbon-loaded foam absorber, and the optical losses (∼10%, scattering and ohmic losses), each effect contributes about a half to the correction factor.

2.2. RF modules

The RF part of the receiver consists of two cartridges, one for each polarization. These cartridges are aligned with dowel pins to the central optical unit. The back plates of the cartridges contain all electrical and mechanical feedthroughs; their mechanical coupling to the mixer module is released during mounting. The cartridges contain all active components from RF couplers and mixers (4 K stage) to IF isolators and HEMT-amplifiers (20 K stage), up to the bias electronics and the servomotors of the mixer backshorts (300 K). With this arrangement, repair and maintenance are easy and decoupled from the optical alignment.

The RF components of the cartridges, such as couplers and mixers, are built in waveguide technology that greatly reduces

space requirements. The mixers are reduced-height waveguide mixers with a single, adjustable, non-contacting backshort (Blundell et al. 1988; Karpov et al. 1998). The current mixing elements are SIS double junctions in Nb technology with individual integrated parallel tuning. Due to the operating frequency below 300 GHz and the junction area >2 μm^2, no magnetic field is required (Winkler & Claeson 1987). Backshort adjustment permits lower sideband (LSB) observing with ~10 dB rejection. This type of mixer performs very well between 210 and 240 GHz, but suffers from low gain at higher frequencies. Wider-band mixers are foreseen for a future upgrade.

The IF signals (3.5–4.5 GHz) of the individual mixers pass cryogenic isolators and are then amplified by 3-stage cryogenic HEMT amplifiers on the 20 K stage (Gallego et al. 1995). A second amplifier stage, close to the cartridges, follows at room temperature before the signals are mixed down to the 0.5 to 1.5 GHz bands and transported via low-loss coax cables to the continuum backends and correlators. The 1-GHz IF bandwith of the system is wide enough to observe simultaneously the ^{13}CO(2–1) and the C^{18}O(2–1) lines at a single frequency setting.

The LO power is generated in a phase-locked Gunn-tripler combination and then split into three branches by a waveguide power splitter. The power of each branch can be adjusted with a resistive vane attenuator. It is then fed by overmoded stainless-steel waveguides to a serial triple-waveguide coupler (3×16 dB) at a temperatue of 4 K. Common LO power adjustment for three mixers does not affect the mixer performance. An optimized power adjustment is pre-registered on lookup tables and the tuning at the telescope is therefore very fast.

The future second polarization module will have an identical but independent LO system that will allow simultaneous multi-frequency observing at 210 to 275 GHz. Since the beams of the two polarization modules coincide, this setup will allow polarimetry by IF correlation. A typical cross polarization of 1% for the corrugated horns, together with the directivity of ~30 dB of the 16 dB couplers, ensures that each polarization unit is isolated by >60 dB from the cross-polarized LO. This value is high enough to ensure that the SIS mixers operate properly.

2.3. Mechanical and cryogenic design

The cryostat is built in stainless steel with an electro-polished interior surface. We designed the cryostat to minimize receiver size and to allow easy access to the interior over various access holes. The cryo-generator is a Daikin closed-cycle refrigerator with two Gifford-McMahon stages (70 K/20 W and 20 K/2 W) and a Joule-Thomson stage for 4 K/1.2 W. The 70 K stage runs from the central optical structure made of aluminum to the shields of the RF cartridges. The 20 K and 4 K stages of the cartridges are coupled via gold-plated, ultra-high purity, solid copper ribbons to the cold heads of the cryo-generator. The three stages of the cartridges are linked together with glass fiber pads concentrically arranged around the optical axis to avoid alignment shifts in the cooled state. We calculated the vertical shift of the central optical unit in the cooled stage and allowed for its effect on the alignment relative to the cryostat window. The complete 70 K exterior surface is covered with a 12-layer super-insulation to reduce radiative thermal losses.

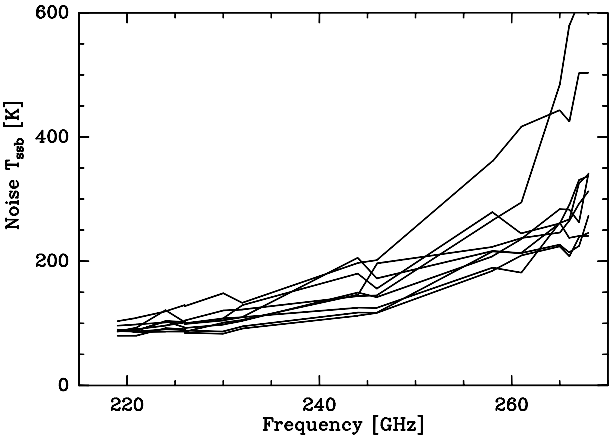

Fig. 2. Single sideband receiver noise temperatures of the 9 receiver elements, measured at the telescope reference plane (Nasmyth Focus).

2.4. System and control

The entire multibeam receiver is controlled by a single VME processor that is located with the ADC and DAC interface boards in a common rack. The system runs under LINUX. The processor board is connected via an Ethernet line to the telescope control system and graphical user interfaces can be exported on remote secured shells. The Ethernet connection is also used to transfer calibrating commands as well as the current elevation and azimuth of the telescope and readings of the temperature sensors. The receiver control program includes the automatic tuning of the LO unit and SIS mixers, the calculated required physical position of the derotator, the conversion of the sensor readings into physical units, and the readings of power meters in the 300 K IF amplifiers. The derotator can be either fixed, or tracking in the horizontal or equatorial coordinate systems with selectable angle offsets.

3. Characteristics at the telescope

We installed HERA at the IRAM 30 m telescope in May 2001. To properly align the cryostat and the derotator, we proceeded as follows. First, we used laboratory antenna-range amplitude and phase curves to precisely measure the position and angle of the central pixel beam emerging from the cryostat window (Carter et al. 2000). Secondly, we made a mechanical mount that allowed us to redefine this optical axis by means of an optical retro-reflector. Next, we installed the cryostat and the retro-reflector at the telescope, and aligned them relative to a laser reference beam mounted on the Nasmyth axis of the 30 m telescope. We then inserted the derotator into the beam, and aligned it so that the retro-reflected laser beam would not vary when the K-mirror was rotated.

At the 30 m telescope, we re-evaluated the receiver noise temperature between 215 and 270 GHz, with independent hot and cold loads at the telescope focal plane. Figure 2 gives the

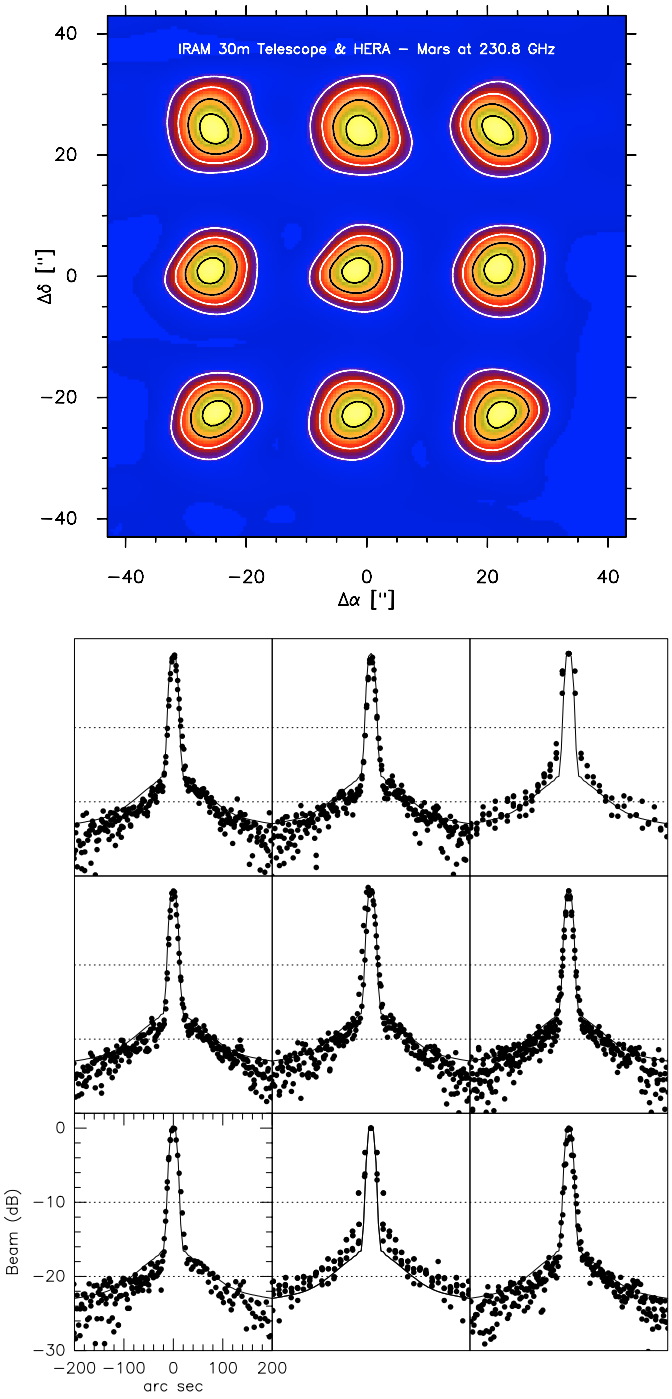

Fig. 3. *Upper panel*: continuum beam map of Mars with active derotation and observing in the beam-chopped, on-the-fly mode. Contours are 15% to 90% of the peak power in 25% steps. *Lower panel*: beam profiles derived from scans across the limb of the moon.

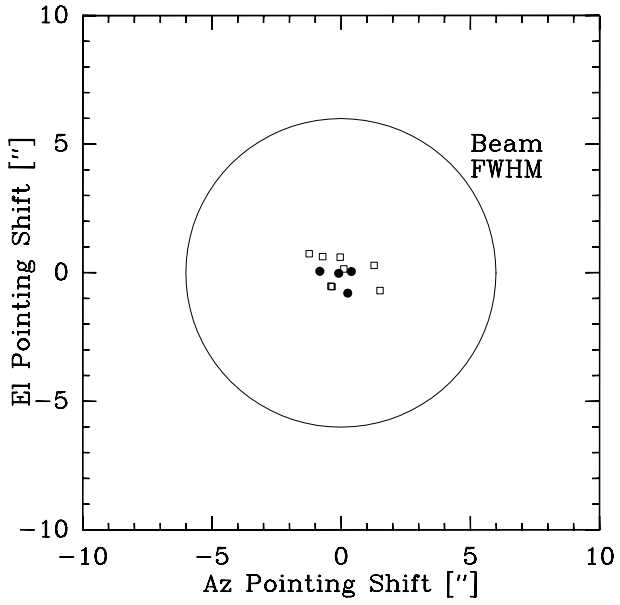

Fig. 4. Pointing toward Uranus with the central pixel; K-mirror in its vertical position (filled points) and from −80° to +80° in 20° steps (320° on sky, empty squares), relative to the 230 GHz beam size.

resulting single sideband noise temperatures of the nine receivers. They are ∼120 K between 215 and 230 GHz, and increase to 200 to 300 K at 270 GHz. The increase in receiver noise at higher frequencies is due to our current mixer design. Future upgrades will use wider-band mixers.

We observed the continuum of the planets to determine the following parameters: common focus for all pixels, beam shapes, and relative position of the beams on the sky. The co-alignment of HERA (central element) with other spectroscopy receivers at the 30 m telescope is better than 5″, a figure that allows us to bootstrap pointing from the lower-frequency receivers, if necessary.

Fits to the individual focussing curves of the nine beams (toward Uranus) gave optimum subreflector adjustments within 0.08 mm. This corresponds to a relative amplitude error of <1% on point sources for a common focus setting. Beam maps of Mars (Fig. 3) gave a beam pattern close to the design goal (cf. Schuster et al. 2000b). The derived beam centroids lay on a regular 24″ grid with a maximum deviation of 0.7″, i.e., within the normal pointing scatter for observing in good weather. For 231 GHz, the mean of the nine beamwidths (*FWHM*) is 11.3″ (range 10.8″ to 11.9″), uncorrected for the size of Mars, which was 5″ during the measurements. The efficiencies as derived from Uranus and Neptune as well as from sky dips gave a sensitivity of 9.6 Jy/K, where temperature is in T_a^* units. The main-beam efficiencies, $B_{\rm eff} = F_{\rm eff}(T_a^*/T_{\rm mb})$, are $B_{\rm eff} = 0.49 \pm 0.04$ for the nine beams, in agreement with the value $B_{\rm eff} = 0.52$ derived from single-beam 230 GHz receivers at the 30 m telescope.

Scans across the limb of the moon were made to measure the error beam in all 9 pixels. Figure 3 shows that the main beam of the nine pixels is clean and that the error beam is below −20 dB, in agreement with the results for single-beam receivers obtained by Greve et al. 1998.

We checked the alignment of the derotator by repeated pointings on the central pixel, with different derotator angles. The data show the K-mirror movement causes a pointing shift of <1″. This is less than a tenth of a beamwidth, so that a special pointing model including the actual derotator position is not required. Together with the high symmetry of the beam pattern on the sky, this low pointing shift allows us to use new

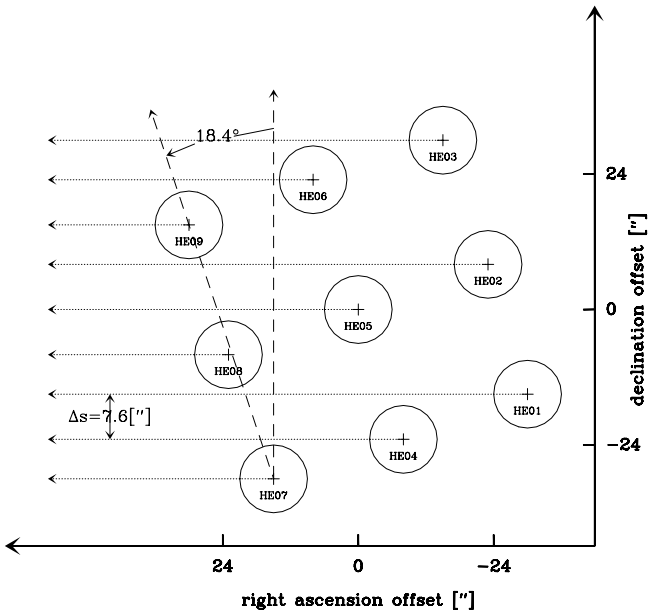

Fig. 5. Example of inclined scanning (Azimuth) with equidistant sampling. The telescope and derotator control allow any other scanning direction. The scanned band has a total width of 68″.

observing schemes, such as fast (<5 s) pixel interchange by rotating the beam pattern by 180°.

Spectral-line observing is possible with the high-resolution autocorrelator VESPA and the 9 × 1 GHz filter bank. All observing modes like position switching, wobbler switching, and frequency switching are possible with HERA using these backends. For small, deep maps, the preferred mode is raster mapping, while for larger maps (>1′−2′), on-the-fly observations are more efficient. Due to the possibility of derotation, these maps can be made with uniform sampling on any user-defined rectangular area, including locally rotated fields. In addition to tracking of the sky rotation, the array can be tilted by specific angles relative to the on-the-fly scanning direction. A relative tilt of ±18.4° ± 90° yields scans with pixels separated by 7.6″, close to full Nyquist sampling (Fig. 5). In this way, a single telescope scan gives a 68″ wide, fully-sampled mapping strip. Finally, the possibility to track the array in azimuth and elevation allows us, if desired, to align the array pattern with the throw direction (azimuth at the 30 m telescope) of the wobbling secondary. By this, wobbling between pixels becomes possible, permitting improved sensitivity for point-source observing.

Due to the reflective optics of HERA, frequency switching yields a clean standing wave pattern with a period of 6.9 MHz (Fig. 6). This period is due to standing waves between the SIS mixers and the telescope secondary. When switching with frequency throws that are multiples of 6.9 MHz, the resulting baselines are very flat (Thum et al. 1995). Frequency throws up to 42 MHz at 10 Hz switching are possible. This mode makes HERA ideal for large-scale mapping of extended galactic clouds for which nearby reference positions are difficult to find. Under good weather conditions ($T_{\rm sys}$ = 250 K) galactic cloud areas as large as 0.5 × 0.5 square degrees can be fully mapped with this mode in roughly 6 h including regular

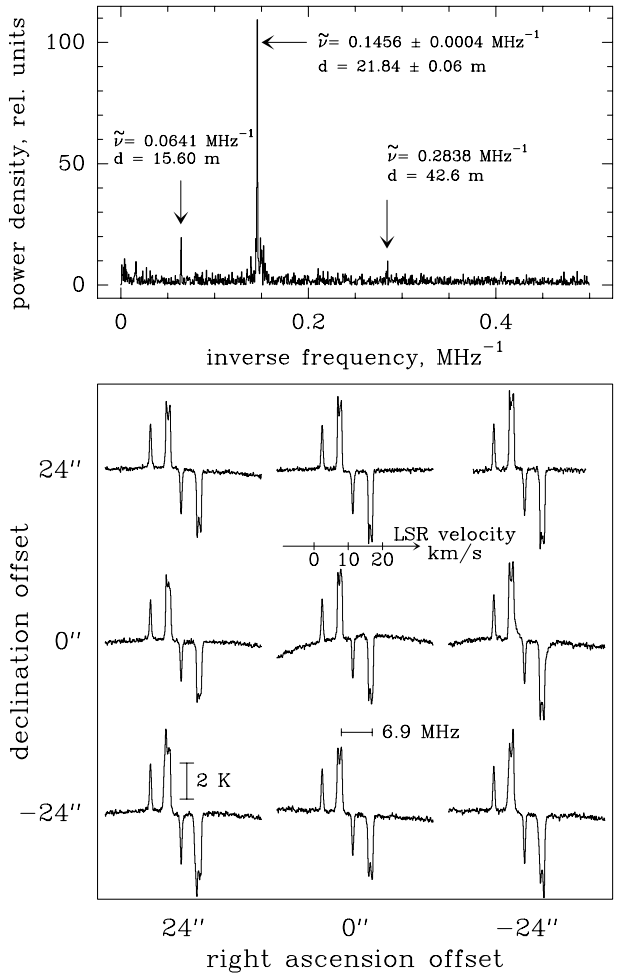

Fig. 6. Spectroscopic baseline ripple. *Upper panel*: Fourier transform of a position-switched observation (the reference position was offset by −1° in elevation), with the central pixel connected to a 1 GHz-wide filter bank. The three ripple components (arrows) have inverse frequencies $\tilde{\nu}$ corresponding to separations d between the reflecting surfaces. *Lower panel*: frequency-switched observations of the dark cloud B133 in the ^{12}CO line at 230.5 GHz, a 5 min integration. The frequency throw was set equal to the dominant ripple frequency (6.9 MHz). The narrow features at 2 and 11 km s^{-1} are mesospheric, the broader features show the opacity and velocity structure of the source. As expected, the baselines are flattest for off-axis pixels.

pointing and focus scans (rms = 0.45 K(T_a^*) per beam for 100 m/s velocity resolution).

The relative calibration among the 9 pixels was measured in spectral mode with the VESPA backend by a simple hot/cold procedure and sequential observation of a common position with all nine beams. The measured relative accuracy was better than 10% (Fig. 7). Most of the remaining uncertainty is due to our currently assumed value of 10 dB for the image band rejection of all mixers. The specific values will be improved in the near future by dedicated sideband calibration hardware. By means of "flat field" observations, the current relative calibration accuracy can be easily improved to better than 1%. For on-the-fly mapping, this implies that striping due to gain calibration errors can be suppressed up to *S/N* ratios of 100 without any other correction schemes or image processing.

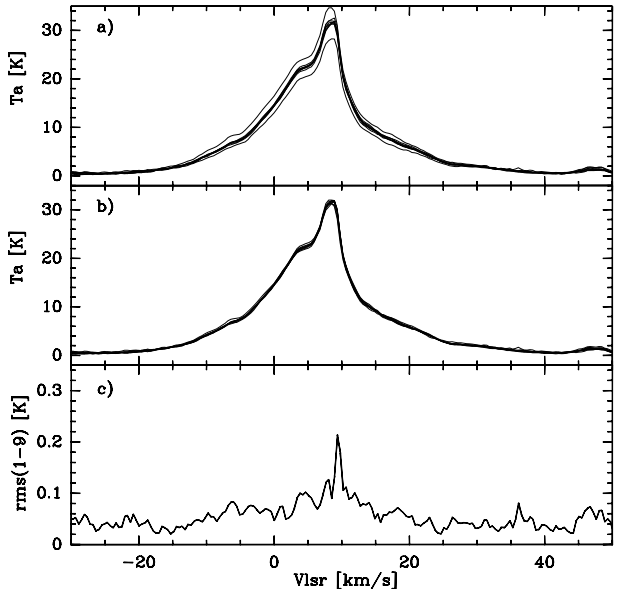

Fig. 7. a) ^{12}CO(2–1) spectra of Orion A, obtained with the nine pixels as a relative calibration check. The array was shifted on a rectangular 24″ grid aligned with the sky coordinates with active field derotation. **b)** Spectra after calibration correction with individual factors obtained from the integrated line fluxes. The identical line shapes mean that pointing errors are negligible. **c)** rms deviation of the temperatures as measured by the different pixels after gain correction.

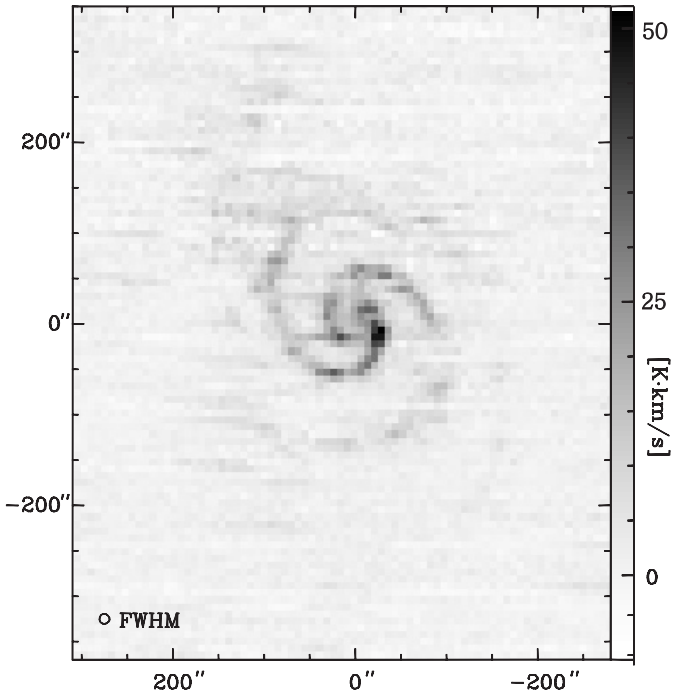

Fig. 8. Velocity integrated CO(2 − 1) emission in M 51, from on-the-fly mapping with an inclined array, scanning in the RA (horizontal) direction. In the vertical direction, the area with Dec offsets −370″ to 0″ was scanned twice (rms 1.4 K km s^{-1}), while the area above Dec offset 0″ was scanned only once (rms 1.8 K km s^{-1}). The total integration time (on and off source) is ∼4 h. The data were corrected for gain drifts with a correlation algorithm. The grey scale shows $\int T_a^* \, dv$.

4. Examples of observations

HERA has now become a facility instrument for astronomers at the 30 m telescope. Pointing and focus scans are usually made with the 9 continuum detectors. With 1 GHz bandwidth, these detectors can also be used for continuum observing with a software interface to the IRAM NIC package. For galactic high-resolution spectral observing and future spectro-polarimetric work, the autocorrelator VESPA is available. Recently a 9 × 1 GHz filter bank (4 MHz resolution) became available and a 9×1 GHz autocorrelator (WILMA, 2 MHz resolution) is nearly completed.

As an example, we show the on-the-fly map of the CO(2–1) emission in M51 (Fig. 8). We made the map in only 4 h with the array tilted at 18.4° to the scan direction (RA). The scanning speed was 3″/s with a sample time of 2 s (6″ in the scan direction). We reduced the map with the 30 m spectral on-the-fly software (Ungerechts et al. 1999). Calibration drifts due to thermal instabilities of the cryo generator and atmospheric fluctuations were corrected by a de-correlation method (Wiesemeyer 2004). The map shows the well-known spiral in the galaxy's inner part (cf. Garcia-Burillo et al. 1993). However the observation shows also that the spiral can be traced much further out, with faint molecular features following the complete outer optical arm in the southwest. The map further reveals for the first time diffuse molecular gas in the northeast, between M51 and its companion, neutral gas that was so far seen only in atomic hydrogen.

5. Summary

We built and installed a new heterodyne multibeam receiver for the 230 GHz band at the IRAM 30 m telescope. The receiver currently runs with 9 single-polarization beams and the second polarization will soon be installed. With typical pixel sensitivities equal to the current single beam instruments at the 30 m telescope, HERA will improve mapping speed by nearly an order of magnitude. Designed as a user instrument, the highly versatile receiver provides unique mapping sensitivity and simplicity of use. Various observing modes including on-the-fly mapping and active field derotation will permit new types of observing projects. The high quality maps will be of great importance as possible zero-spacing data for millimeter interferometers. Future extensions of the instrument will include polarization mapping and large-bandwidth, optimum-sensitivity point source observations.

Acknowledgements. We thank the staff from IRAM Granada and IRAM Grenoble for their continued support and the excellent quality of their work. Y. Bortolotti, F. Morel, G. Butin, S. Halleguen and D. Billon-Pierron provided important components to the system and F. Mattiocco helped with the high frequency characterization of the waveguide components. P. Hily-Bland and P. Planesas helped with the commissioning of the instrument. In its early phase the project received important input and advice from J. Lamb. D. Downes greatly helped to improve the manuscript. We thank the anonymous referee for valuable comments.

References

Blundell, R., Carter, M. C., & Gundlach, K. H. 1988, Int. J. Infrared and Millimeter Waves, 9, 361

Brüll, M. 2000, Diploma Thesis, Feb., I. Physikalisches Institut der Universität zu Köln

Garcia-Burillo, S., Guelin, M., & Cernicharo, J. 1993, A&A, 274, 123

Carter, M., Baryshev, A., Hesper, R., et al. 2002, 13th Int. Symp. Space Terahertz Techn. Proc., Cambridge, Mass., 515

Gallego, J. D. 1995, Tech. Report CAY 1995-3, Centro Astronomico de Yebes

Gear, W. K., & Cunningham, C. R. 1995, in Multifeed Systems for Radio Telescopes, ed. D. T. Emerson, & J. M. Payne, ASP Conf. Ser., 75, 215

Graf, U. U., Heyminck, S., Michael, E. A., et al. Proc. SPIE, 4855, Waikoloa, Hawaii

Greve, A., Kramer, K., & Wild, W. 1998, A&AS, 133, 271

Karpov, A., Blondel, J., Carter, M., Billon-Pierron, D., & Gundlach, K. H. 1998, Int. J Infrared and Millimeter Waves, 19, 117

Klein, T., Güsten, R., Gueth, F., et al. Proc. SPIE, 4855, Waikoloa, Hawaii

Poglitsch, A., Beeman, J. W., Geis, N., et al. 1991, Int. J Infrared and Millimeter Waves, 12, 859

Schuster, K.-F., Blondel, J., Carter, M., et al. 2000a, in Imaging at Radio through Submillimeter Wavelengths, ed. J. M. Mangum, & S. J. E. Radford, ASP Conf. Ser., 217, 25

Schuster, K., Blondell, J., Carter, M., et al. 2000b, Proc. SPIE, 4015, Munich

Sunada, K., Yamaguchi, C., Nakai, N., et al. 2000, Proc. SPIE, 4015, Munich

Thum, C., Sievers, A., Navarro, S., Brunswig, W., & Penãlver, J. 1995, IRAM Working Report No. 228/95

Ungerechts, H., Brunswig, W., Kramer, C., et al. 1999, 30 m Telescope Spectral On-The-Fly Mapping, `www.iram.es/OTF/HTML/sl-otf.html`

Wiesemeyer, H., et al. 2004 in preparation

Winkler, D., & Claeson, T. 1987, J. Appl. Phys., 62, 4482